One-phonon resonant Raman scattering in $Al_xGa_{1-x}As$ ($0.5 < x < 0.7$): Dipole-forbidden Fröhlich interaction and interference effects

C. Trallero-Giner,* A. Cantarero,† and M. Cardona
Max-Planck-Institut für Festkörperforschung, Heisenbergstrasse 1, D-7000 Stuttgart 80, Federal Republic of Germany

V. I. Gavrilenko
Institute of Semiconductors, Ukrainian Academy of Science, pr. Nauki 115, 252650 Kiev-28, U.S.S.R.
(Received 20 August 1990)

The dipole-forbidden resonant Raman scattering by LO phonons via Fröhlich interaction and the corresponding interference effects with allowed scattering are studied near the E_0 gap of $Al_xGa_{1-x}As$ alloys at 100 K. Three high-purity n-type $Al_xGa_{1-x}As$ samples covering the aluminum content $0.5 < x < 0.7$ were investigated. A theoretical model of Fröhlich-interaction-induced resonant Raman scattering by one LO phonon including excitonic effects has been considered. Alloy effects have been taken into account in the Raman polarizability through a virtual-crystal approximation by including the compositional dependence of the parameters used in the theory (energy gap, effective mass, exciton Rydberg, etc.) and exciton lifetime broadening. The measured absolute values of the dipole-forbidden Raman polarizability for both GaAs and AlAs modes are in good agreement with the calculated ones for the three alloy compositions studied. Interference between the dipole-forbidden and dipole-allowed Raman scattering is clearly seen for both GaAs and AlAs modes in the whole compositional range measured. The theoretical curves reproduce the principal features of the measured interference resonant Raman profile. Comparison between the different $Al_xGa_{1-x}As$ samples shows that an aluminum concentration $x > 0.5$ enhances the extrinsic dipole-forbidden Raman scattering by LO phonons.

I. INTRODUCTION

It is well known that the vibrational properties of $Al_xGa_{1-x}As$ reveal a two-mode behavior of the LO phonon: in the range $0.1 < x < 0.9$ there are GaAs- and AlAs-like modes.[1-3] The normalized Raman scattering intensity in the neighborhood of the E_0 gap has been reported in Ref. 1 for $x = 0.43$ and 0.48. Recently, in Refs. 4 and 5 the absolute efficiencies for dipole-allowed resonant Raman scattering (RRS) by LO phonons have been studied for an aluminum content in the range $0.2 < x < 0.7$. It was shown that a theory for the one-phonon RRS which includes excitons as intermediate states and the effect of alloying through a virtual-crystal approximation (VCA) can reproduce the resonant profiles in the $Al_xGa_{1-x}As$ alloys.[5] In this theoretical model the exciton lifetime was used as a fitting parameter; in this way the different broadening effects related to disorder and intervalley exciton scattering are included in an *ad hoc* manner as a function of aluminum concentration. The results obtained show that the lifetime has a linear dependence on x within the range $0 < x < 0.49$ while for $x > 0.45$ a rapid superlinear increase with x is observed.[5]

In the present paper we report the absolute values of the Raman tensor, including dipole-forbidden and interference effects, for RRS by LO phonons near the E_0 gap of $Al_xGa_{1-x}As$ alloys in the x range $0.5 < x < 0.7$. In order to compare the experimental data obtained with the theoretical results,[6] the Fröhlich interaction has been generalized for alloys by means of a phenomenological virtual-crystal approach.

It has been shown for bulk semiconductors that besides the dipole-forbidden scattering by LO phonons via Fröhlich interaction, a second forbidden mechanism is not necessary in order to fit the resonance profiles when excitonic effects are considered.[6] We need, however, a second mechanism for the $Al_xGa_{1-x}As$ alloys; the exciton created by the incoming light is scattered by the Fröhlich and also by another mechanism, which can be assumed to be impurity-induced Fröhlich interaction. Here this mechanism has been included in a simple way by assuming that its Raman polarizability is proportional to the pure dipole-forbidden Fröhlich interaction but incoherent. The relative strength of the intensity due to the intrinsic and "extrinsic" dipole-forbidden Raman scattering by LO phonons can be obtained by fitting the measured resonance profiles.

II. EXPERIMENTAL PROCEDURE

Three high-purity $Al_xGa_{1-x}As$ samples covering the aluminum content $0.5 < x < 0.7$ were investigated. The characteristics of the different samples, the estimated aluminum content, and the procedure to obtain absolute values for the squared Raman polarizabilities are summarized in Ref. 5.

The measurements were performed in backscattering geometry on a (001) surface. We denote by x, y, z, x', and y' the [100], [010], [001], [110], and [1$\bar{1}$0] directions, respectively.

For backscattering on a (001) surface the Raman tensor for scattering by one LO phonon can be written as follows:[7] (i) dipole-allowed scattering via deformation-potential interaction

$$\vec{\vec{R}}_{\mathrm{DP}}=\begin{pmatrix} 0 & a_{\mathrm{DP}} & 0 \\ a_{\mathrm{DP}} & 0 & 0 \\ 0 & 0 & 0 \end{pmatrix}, \tag{1}$$

(ii) dipole-forbidden scattering via Fröhlich interaction

$$\vec{\vec{R}}_{F}=\begin{pmatrix} a_F & 0 & 0 \\ 0 & a_F & 0 \\ 0 & 0 & a_F \end{pmatrix}, \tag{2}$$

(iii) extrinsic-induced dipole-forbidden scattering via Fröhlich interaction

$$\vec{\vec{R}}_{\mathrm{Fe}}=\begin{pmatrix} a_{\mathrm{Fe}} & 0 & 0 \\ 0 & a_{\mathrm{Fe}} & 0 \\ 0 & 0 & a_{\mathrm{Fe}} \end{pmatrix}, \tag{3}$$

where a_{DP}, a_F, and a_{Fe} are the corresponding Raman polarizabilities. The squared Raman tensors projected into the following four different backscattering configurations $|\mathbf{e}_s\cdot\vec{\vec{R}}\cdot\mathbf{e}_l|^2$ are

$$\begin{aligned}
&\text{I: } \bar{z}(x',x')z, \quad |a_F+a_{\mathrm{DP}}|^2+|a_{\mathrm{Fe}}|^2 ; \\
&\text{II: } \bar{z}(y',y')z, \quad |a_F-a_{\mathrm{DP}}|^2+|a_{\mathrm{Fe}}|^2 ; \\
&\text{III: } \bar{z}(x,x)z, \quad |a_F|^2+|a_{\mathrm{Fe}}|^2 ; \\
&\text{IV: } \bar{z}(y,x)z, \quad |a_{\mathrm{DP}}|^2 .
\end{aligned} \tag{4}$$

The scattering by LO phonons via deformation-potential and Fröhlich interactions are mutually coherent processes. The extrinsic Fröhlich scattering (or another mechanism due to disorder) leads to a manifold of final states in $\mathbf{q}$ space ($\mathbf{q}$ is the phonon wave vector). From a quantum-mechanical point of view the above processes correspond to a mixed ensemble and the total probability should be the sum of the probabilities of the corresponding pure ensembles. In this way the scattering intensity of the extrinsic Fröhlich scattering has to be added to the intensity of the corresponding intrinsic processes.

III. THEORY OF RAMAN POLARIZABILITY IN $Al_xGa_{1-x}As$ ALLOYS

A quantum-mechanical treatment of RRS for exciton–one-phonon Fröhlich and deformation-potential interactions in pure semiconductors with diamond and zinc-blende structure has been given earlier.[6,8] In the following we outline a model for the Raman polarizabilities of $Al_xGa_{1-x}As$ alloys when the exciton–one-phonon interaction is given by the Fröhlich Hamiltonian. As in Ref. 5 we use a VCA, where the unit cell has an effective volume $(1-x)V_c$ for the GaAs mode and xV_c for the AlAs mode, V_c being the volume of the unit cell. This model permits us to treat the Raman polarizability by partly localized GaAs and AlAs modes in the same way as that of phonons in perfect bulk semiconductors. Considering intermediate electronic states as excitonic states and using the results of Ref. 6, the Raman polarizability is given by

$$\begin{aligned}
a_F=\sum_p K_p^F\Bigg[&\sum_{n,m=1}^{\infty}\frac{D_{n,m}}{(\eta_p+1/n^2+i\gamma_p)(\eta_p-\eta_0+1/m^2+i\gamma_p)} \\
&+\sum_{n=1}^{\infty}\frac{1}{n^3}\int_0^{\infty}dk\,\frac{D_{n,k}}{1-e^{-2\pi/k}}\Bigg[\frac{1}{(\eta_p+k^2+i\gamma_p)(\eta_p-\eta_0+1/n^2+i\gamma_p)} \\
&\qquad+\frac{1}{(\eta_p+1/n^2+i\gamma_p)(\eta_p-\eta_0-k^2+i\gamma_p)}\Bigg] \\
&+\frac{i}{8(Q_e^2-Q_h^2)}\Bigg[\frac{1}{Q_e}\ln\frac{\sqrt{\eta_p+i\gamma_p}+\sqrt{\eta_p-\eta_0+i\gamma_p}-Q_e}{\sqrt{\eta_p+i\gamma_p}+\sqrt{\eta_p-\eta_0+i\gamma_p}+Q_e} \\
&\qquad-\frac{1}{Q_h}\ln\frac{\sqrt{\eta_p+i\gamma_p}+\sqrt{\eta_p-\eta_0+i\gamma_p}-Q_h}{\sqrt{\eta_p+i\gamma_p}+\sqrt{\eta_p-\eta_0+i\gamma_p}+Q_h}\Bigg]\Bigg]+b_F ,
\end{aligned} \tag{5}$$

where $Q_\alpha=(m_\alpha/m_T)qa$ $(\alpha=e,h)$, $m_T=m_e+m_h$, m_e (m_h) is the electron (hole) effective mass, and a is the exciton Bohr radius. The terms $D_{n,m}$ and $D_{n,k}$ are calculated in Ref. 6. The coefficient K_p^F in Eq. (5) is given by

$$K_p^F=\sqrt{f}\,\frac{2}{\pi}\left[a_0^3(x)\frac{M^*}{m_0}\frac{\hbar\omega_0(x)}{R_H}\right]^{1/2}\frac{q(x)a_H}{\hbar\omega_l\sqrt{\hbar\omega_l\hbar\omega_s}}\,\frac{2}{3}\,\frac{|P|^2}{m_0}$$
$$\times\frac{a_H}{a(x)}\,\frac{R_H^2}{R^2(x)}C_F^*(x)\frac{m_e(x)-m_h(x)}{m_T(x)}\,, \tag{6a}$$

$$C_F=-i\left[2\pi\hbar\omega_0(x)e^2\left[\frac{1}{\epsilon_\infty}-\frac{1}{\epsilon_0}\right]\right]^{1/2}$$
$$=\frac{-e_T e}{\epsilon_\infty}\left[\frac{8\pi^2\hbar^2}{V_c M^*\omega_0}\right]^{1/2}, \tag{6b}$$

ϵ_0 and ϵ_∞ being the static and ir dielectric constants, respectively, e_T the transverse charge, a_0 the unit cell parameter, ω_0 the phonon frequency, R_H and a_H are the Rydberg and Bohr radius of the hydrogen atom, m_0 the electron mass, and $P=\langle s|p_x|x\rangle$ the matrix element of the momentum operator. The reduced mass of the primitive cell M^* is taken to be $M^*_{\rm GaAs}$ for the GaAs mode and $M^*_{\rm AlAs}$ for the AlAs mode. This choice differs from previous calculations[5,6] where a mean value $M^*(x)$ was taken for both modes. However, the present choice is more consistent with a VCA, where we consider our crystal as built up from two bulk materials (AlAs and GaAs) with different percentages, although we must keep in mind that our modes are normal modes corresponding to both portions of the crystal. The index p refers to the exciton formed between a valence and a conduction band with gap E_{gp}, and

$$\eta_p=\frac{\hbar\omega_l-E_{gp}}{R},\quad \eta_0=\frac{\hbar\omega_0}{R},\quad \gamma_p=\frac{\Gamma_p}{R}\,, \tag{7}$$

Γ_p being the exciton lifetime broadening and R the exciton Rydberg. The coefficient f in Eq. (6) is the fraction of atoms per unit cell of Al for the AlAs mode and of Ga for the GaAs mode. The term b_F corresponds to the contribution of other nonresonant diagrams.

The first term on the right-hand side of Eq. (5) corresponds to transitions to discrete exciton states, the second and third terms to discrete-continuous and continuous-discrete states, while the last term is the contribution only from the continuum in which the wave functions have been taken to be the uncorrelated electron-hole pairs in order to simplify the calculation.

The Raman polarizability for deformation-potential interaction in $Al_xGa_{1-x}As$ alloys as obtained in Ref. 5 using a three-band model is

$$a_{\rm DP}=\sum_{p,q}K_{p,q}(x)\left\{\sum_{n=1}^{\infty}\frac{1}{2n^3}\frac{1}{(\eta_p+1/n^2+i\gamma_p)(\eta_q-\eta_0+1/n^2+i\gamma_p)}\right.$$
$$+\frac{1}{4[\eta_0+\eta_p-\eta_q+i(\gamma_p-\gamma_q)]}$$
$$\left.\times\left[\ln\frac{\eta_q-\eta_0+i\gamma_q}{\eta_p+i\gamma_q}+\pi i\left[\coth\frac{\pi}{\sqrt{\eta_p+i\gamma_p}}-\coth\frac{\pi}{\sqrt{\eta_q-\eta_0+i\gamma_q}}\right]\right]\right\}. \tag{8}$$

The coefficient $K_{q,p}$ is equal to

$$K_{q,p}=\sqrt{f}\,\frac{a_0^2(x)}{2\pi m_0}\,\frac{R_H^2}{\sqrt{3}R^2(x)}\left[\frac{a_H}{a(x)}\right]^3$$
$$\times\frac{d_0|P|^2}{\hbar\omega_l\sqrt{\hbar\omega_l\hbar\omega_s}}C_{p-q}\,, \tag{9}$$

where d_0 is the optical deformation-potential constant. The sum in p and q runs over heavy (hh), light (lh) holes, and split-off (so) valence bands.

The coefficient C_{p-q} is a numerical factor that represents the weight of different band transitions. Mean values of calculated C_{p-q}'s are given in Table II of Ref. 5. For low-impurity concentration the impurity-induced dipole-forbidden scattering by LO phonons can be calculated using fourth-order perturbation theory. An expression for the Raman scattering efficiency $dS/d\Omega$ that includes only the discrete exciton states has been given in Ref. 9. The transitions belonging to different virtual exciton states (two discrete virtual states and one in the continuum, two states belonging to the continuum and one to the discrete spectrum and the contribution of the continuous spectrum only) give an important contribution to the absolute value of $a_{\rm Fe}$, which we take to be

$$|a_{\rm Fe}|^2=\alpha^2|a_F|^2\,, \tag{10}$$

where α is an adjustable parameter.

IV. RESULTS AND FITTING PROCEDURE

Figure 1 depicts the resonance of the dipole-forbidden Raman scattering by LO phonons near the E_0 gap for the three $Al_xGa_{1-x}As$ samples studied in the compositional range $0.5<x<0.7$ [$\bar{z}(x,x)z$ configuration]. The dipole-allowed results [$\bar{z}(y,x)z$] have been recalculated with the new reduced masses and are also presented in Fig. 1. The solid and dashed thick lines are fits to the experimental points.

Figure 2 shows the interference of both mechanisms measured in the configuration I and II of Eq. (4) for $x=0.555$, 0.62, and 0.69, including both GaAs and AlAs modes. The thick lines represent the theoretical fits. The interference effects persist in the whole composition range studied for both LO-phonon modes. It can be seen from Figs. 1 and 2 that the E_0 gap increases with higher Al concentration and at the same time that the heights of the resonance profiles decrease as the increasing widths increase. The heights of the resonance profiles decrease faster for the GaAs modes than for AlAs modes and $|a_{\mathrm{GaAs}}|^2$ is smaller than $|a_{\mathrm{AlAs}}|^2$ for the three Al concentrations measured.

The experimental spectra of $|a|^2$ for the configurations given in Eq. (4) have been compared with the calculation based on Eqs. (5), (8), and (10) for resonance scattering by LO phonons near the E_0 gap. For the material parameters of $Al_xGa_{1-x}As$ we take lattice constant[3]

$$a_0(x)=5.6533+0.0078x \text{ Å} ; \tag{11}$$

exciton Rydberg[5]

$$R(x)=4.45+6.82x+5.48x^2 \text{ meV} ; \tag{12}$$

exciton Bohr radius[5]

$$a(x)=122-142x+61x^2 \text{ Å} ; \tag{13}$$

effective masses[3]

$$\frac{m_e(x)}{m_0}=0.067+0.083x \quad \text{(electron mass)} , \tag{14a}$$

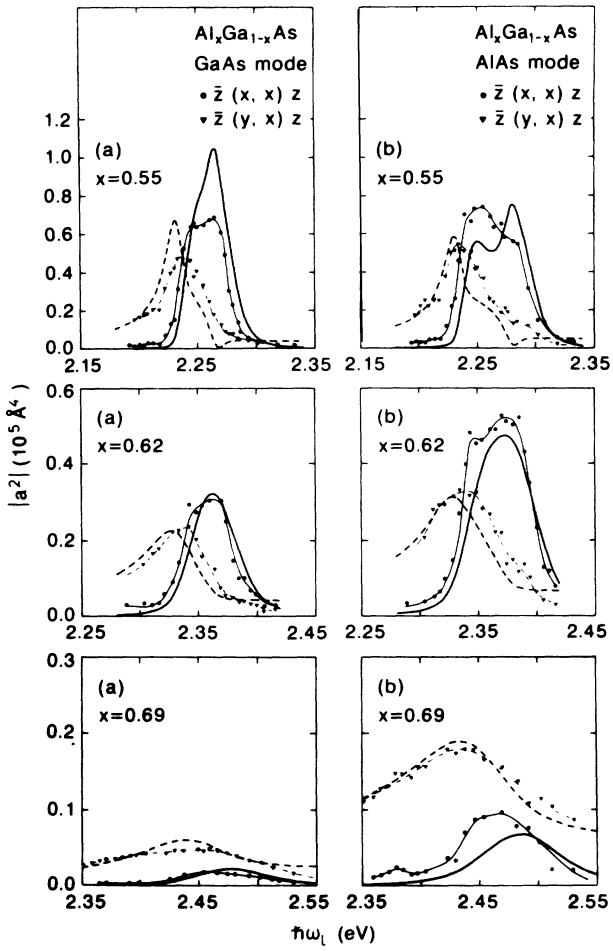

FIG. 1. Squared Raman polarizability for allowed deformation potential and dipole-forbidden scattering by LO phonons measured in $Al_xGa_{1-x}As$ at 100 K with $x=0.555$, 0.62, and 0.69. The thick solid lines are fits with Eqs. (5), (6), and (10) for forbidden scattering (expt., dots) while the thick dashed lines represent the calculation for deformation potential scattering (expt., triangles). (a) GaAs mode, (b) AlAs mode. The solid and dashed thin lines are a guide to the eye representing the experimental points.

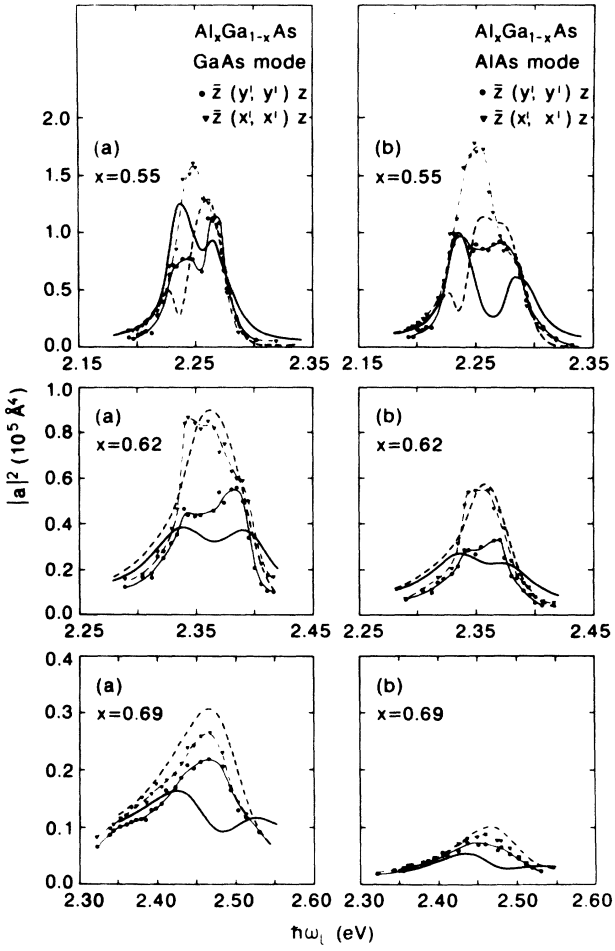

FIG. 2. Squared Raman polarizabilities for scattering by LO phonons in $Al_xGa_{1-x}As$ (001) at 100 K measured with $\mathbf{e}_l \| \mathbf{e}_s$ [configuration I of Eq. (4) triangles, configuration II dots] for $x=0.555$, 0.62, and 0.69. The thick dashed lines are fits with Eqs. (5), (6), and (10) for configuration I, thick solid lines for configuration II. (a) GaAs mode, (b) AlAs mode. The solid and dashed thin lines are a guide to the eye representing the experimental points.

$$\frac{m_{\rm lh}(x)}{m_0}=0.087+0.063x \quad \text{(light hole)}, \tag{14b}$$

$$\frac{m_{\rm hh}(x)}{m_0}=0.62+0.14x \quad \text{(heavy hole)}, \tag{14c}$$

$$\frac{m_{\rm so}(x)}{m_0}=0.15+0.09x \quad \text{(split-off hole)}; \tag{14d}$$

E_0 critical-point energy[5]

$$E_g(x)=1.510+1.115x+0.37x^2 \text{ eV}; \tag{15}$$

phonon frequencies[5]

$$\hbar\omega_0^{\rm GaAs}=31.62+4.58(1-x) \text{ meV}, \tag{16a}$$

$$\hbar\omega_0^{\rm AlAs}=45.3+4.7x \text{ meV}; \tag{16b}$$

exciton broadening $\Gamma_p=\Gamma_q$, $\Gamma_0(x)$ from Ref. 5,

$$\Gamma_0(x)=4.02+1172.92(x-0.49)^2 \text{ meV}, \quad 0.49<x<0.7; \tag{17}$$

and static and high-frequency dielectric constants[3]

$$\epsilon_0(x)=13.18-3.12x, \tag{18a}$$

$$\epsilon_\infty(x)=10.84-2.73x. \tag{18b}$$

In order to evaluate the scattering wave vector q, which appears in the dipole-forbidden Raman polarizability, we used the expression $q=(n/c)(\omega_l+\omega_s)$ with $n(\omega)\simeq\sqrt{\epsilon_1(\omega)}$, where[10]

$$\epsilon_1(\omega)=A_0(x)\{f(x)+\tfrac{1}{2}\{E_g(x)/[E_g(x)+\Delta_0]\}^{3/2}f(x_{\rm so})\}+\beta_0(x); \tag{19}$$

$$f(\chi)=\chi^{-2}[2-(1-\chi)^{1/2}-(1-\chi)^{1/2}]; \tag{20}$$

$$\chi=\hbar\omega/E_g(x), \quad \chi_{\rm so}=\hbar\omega/[E_g(x)+\Delta_0]; \tag{21}$$

$$A_0(x)=6.3+19.0x, \quad \beta_0(x)=9.4-10.2x. \tag{22}$$

The calculations have been performed with the parameters obtained from Eqs. (11)–(22). A small background of 10 and 20 Å (corresponding to GaAs and AlAs modes) has been added in the theoretical curves corresponding to $x=0.69$. In all samples studied the value used for d_0 is 36 eV (Ref. 11) and $|P|^2/m=12.9$ eV.[9]

The dipole-forbidden and the interference curves were fitted with the broadening Γ_0 determined from the deformation potential resonance.[5] The prefactor α in Eq. (10) for the extrinsic dipole-forbidden Raman scattering was adjusted for each spectrum to reach the maximum measured total $|a|^2$. The best fits in Fig. 1 are obtained for $\alpha=|a_{\rm Fe}|^2/|a_F|^2=0.56$, 1.5, and 1.5 for $x=0.555$, 0.62, and 0.69, respectively. This means that of the total dipole-forbidden Raman scattering about 64% for the sample 1, 40% for the samples 2 and 3, is due to the intrinsic Fröhlich mechanism. The small value of α for x close to 0.5 is not easy to understand since for this composition the alloy potential fluctuations should be the largest.

It can be seen in Fig. 1 that the calculated dipole-forbidden scattering (thick dashed lines) is slightly but systematically shifted to higher energy with respect to the experimental data, while the theoretical values corresponding to the dipole-allowed case are shifted to lower energies. These minor discrepancies cannot be understood in the framework of the theory presented here. The calculated interference curves displayed in Fig. 2 reproduce qualitatively the principal features of the measured Raman constructive and destructive interferences for both GaAs and AlAs modes. As in Fig. 1, when the Al concentration increases the intensity of interferences for both modes decreases, but the intensity of the AlAs mode decreases more slowly than that of the GaAs mode. The calculated maximum in the constructive and destructive interferences is also shifted with respect to the measured ones. The theoretical values corresponding to configuration II agree worse with the experimental results than those for configuration I. A calculation of impurity-induced Fröhlich interaction, including excitonic effects, should give a better fit of the resonance profile of the interference curves. Nevertheless, the order of magnitude and the principal features of the one-phonon RRS in $Al_xGa_{1-x}As$ alloys can be obtained with the excitonic theory presented in Sec. III.

V. CONCLUSIONS

Absolute values of dipole-forbidden Raman scattering by LO phonons and its interference with the dipole-allowed mechanism near resonance with the E_0 gap of $Al_xGa_{1-x}As$ have been measured for $0.5<x<0.7$. Theoretical models for the Fröhlich interaction and the extrinsic q-induced Raman scattering, including exciton states as intermediate states and the alloying effects in the Raman tensor through a generalized VCA, reproduce quite well the dipole-forbidden resonant profiles. We have shown that the interference of dipole-allowed and dipole-forbidden Raman scattering by LO phonons persists near the E_0 gap. The principal characteristics of the interference resonant profiles for both phonon modes in $Al_xGa_{1-x}As$ alloys are reproduced by the theory. The strengths of the intrinsic dipole-forbidden Raman scattering decrease as the aluminum content increases, due to an increase in lifetime broadening.

ACKNOWLEDGMENTS

C.T.-G. and A.C. thank the Alexander von Humboldt Foundation and the Ministerio de Educación y Ciencias of Spain, respectively, for financial support. Thanks are also due to E. Bauser for the preparation of the samples.

*Permanent address: Department of Theoretical Physics, Havana University, San Lazaro y L, Havana, Cuba.

†Permanent address: Departament de Física Aplicada, Universitat de València, 46100-València, Spain.

[1]J. Shah, A. E. DiGiovanni, T. C. Damen, and B. I. Miller, Phys. Rev. B **7**, 3481 (1973).

[2]B. Jusserand and R. Bonneville, Physica B **117&118**, 365 (1983).

[3]S. Adachi, J. Appl. Phys. **58**, R1 (1985).

[4]V. I. Gavrilenko, C. Trallero-Giner, M. Cardona, and E. Bauser, Solid State Commun. **67**, 459 (1988).

[5]C. Trallero-Giner, V. I. Gavrilenko, and M. Cardona, Phys. Rev. B **40**, 1238 (1989).

[6]C. Trallero-Giner, A. Cantarero, and M. Cardona, Phys. Rev. B **40**, 4030 (1989).

[7]M. Cardona, in *Light Scattering in Solids II,* Vol. 50 of *Topics in Applied Physics,* edited by M. Cardona and G. Güntherodt (Springer, Berlin, 1982), p. 19.

[8]A. Cantarero, C. Trallero-Giner, and M. Cardona, Phys. Rev. **39**, 8388 (1989).

[9]A. Alexandrou, C. Trallero-Giner, A. Cantarero, and M. Cardona, Phys. Rev. B **40**, 1603 (1989).

[10]S. Adachi, J. Appl. Phys. **53**, 5863 (1982).

[11]A. Blacha, H. Presting, and M. Cardona, Phys. Status Solidi B **126**, 11 (1984).